applied sciences

MDPI

Article

A New Method to Determine the Steel Fibre Content of Existing Structures—Test Setup and Numerical Simulation

Simon Cleven *, Michael Raupach and Thomas Matschei

Institute of Building Materials Research, RWTH Aachen University, Schinkelstr. 3, 52062 Aachen, Germany; raupach@ibac.rwth-aachen.de (M.R.); matschei@ibac.rwth-aachen.de (T.M.)
* Correspondence: cleven@ibac.rwth-aachen.de; Tel.: +49-241-8095-113

Abstract: The diagnostics of constructions built with steel fibre reinforced concrete are extremely difficult to conduct because, typically, no information on the actual amount and orientation of the fibres is available. Therefore, it is of great interest to engineers to have the possibility to determine the steel fibre content and, at best, also the orientation of the fibres in existing structures. For this purpose, an easy-to-use test setup was developed and tested, in the course of laboratory investigations. This method can be used for cylinders, for example drilling cores, that can later be taken of existing structures, to determine both the fibre content and orientation. Based on these results, a model for cylindrical specimens was derived, which can be used for varying concrete compositions with steel fibre contents of up to 80 kg/m^3. In the case of missing information concerning the concrete composition, it allows an initial estimation for the fibre content. In case additional information about the concrete composition is available, a much higher accuracy of the projected steel fibre content and therefore, an assessment of the building's condition is possible.

Keywords: steel fibre reinforced concrete; electrical resistivity; fibre content; non-destructive test method

Citation: Cleven, S.; Raupach, M.; Matschei, T. A New Method to Determine the Steel Fibre Content of Existing Structures—Test Setup and Numerical Simulation. *Appl. Sci.* **2022**, *12*, 561. https://doi.org/10.3390/app12020561

Academic Editors: José A. F. O. Correia, Gabriele Bertagnoli and Diego Gino

Received: 3 December 2021
Accepted: 5 January 2022
Published: 6 January 2022

1. Introduction

Short fibres, especially steel fibres, can be used for the reinforcement of concrete to increase ductility, toughness, resistance to cracking and tensile strength (see, e.g., [1–6]). As a consequence, it is possible to reduce or even avoid the use of traditional reinforcements. The mechanical properties of steel fibre reinforced concretes (SFRCs) are highly dependent on the fibre content and the fibre distribution and orientation inside the concrete elements (see, e.g., [1,7,8]). Areas with a very low number of fibres or fibres that are not oriented in the direction of the tensile tension lead to a higher risk of cracking and can cause the failure of the whole structure (see, e.g., [9,10]). For this purpose, during the casting of SFRC, significant quality control measures, e.g., the regular testing of the amount of steel fibres by wash out procedures, need to be applied. Assuming an optimum concrete composition, SFRC typically possesses a longer service life and thus, a lesser need for maintenance. This makes it an interesting material for the repair of reinforced concrete structures (see, e.g., [4,11]). Nevertheless, in the case of SFRC application, the real fibre content and, especially, the fibre distribution are not well known and so, the use of significant safety factors is necessary during the design stage (see, e.g., [12–15]).

These problems show the need for a test setup that is easy to apply, ideally non-destructive and can be used for rehabilitation processes to determine the fibre parameters, for example (see, e.g., ([16–19]). Possible methods that were used in different studies are based on computer tomography (CT), microscopic analysis of sectional images or inductivity measurements (see, e.g., [10,17,18,20–26]). The main problems with CT analysis are its high cost and the limited size of specimens. Furthermore, it is not possible to use this technique in situ on construction sites. The same arguments can be found for cross sectional image analysis, whereas this technique is even less accurate than CT scanning. Inductive techniques are easier to use but are also limited to small specimen sizes.

A technique that is already used for structural concrete monitoring to identify and locate steel rebars is the electric resistivity measurement (see, e.g., [27–32]. Based on an easy-to-use test setup, which was already tested in past studies conducted by the authors [33], a new application test based on the analysis of cylindrical specimens is proposed in this research paper. In the first part of the study, the test setup is adjusted and a numerical model is generated to simulate the flow of the alternating current, which enables the comparison and calculation of the resistivity of the different specimen directions that are possible. With help of the proposed setup, cylindrical specimens with fibre contents of up to 80 kg/m^3 are analysed and correlations between the electrical resistivity and the fibre content and fibre orientation are developed to enable the use of drilling core samples in the second part [34].

2. Materials and Methods

2.1. Concrete Mix Design

The concrete used in all experiments was the same mixture, which was also used in [33]. It was designed for a good workability, even at high fibre contents, and adherence to the regulations of EN 206 [35]. To investigate both plain concrete (PC) and steel fibre reinforced concrete (SFRC), the basic concrete mix design, shown in Table 1, was used for all mixes. Fibre dosages of 40 kg/m^3 and 80 kg/m^3 were used, respectively. The macro steel fibre was produced from steel wire with hooked ends and had a length of 60 mm and a diameter of 1 mm, which equals an aspect ratio of 60.

Table 1. Concrete mix design of the basic concrete.

Parameter	Unit	32–60–300–00
CEM I 32.5 R	kg/m^3	300.0
Water	kg/m^3	180.0
Aggregates	kg/m^3	1849.5
Water/cement ratio	-	0.60
Grain size distribution	-	A/B16
Steel fibre type	-	Macrofibre 60 mm
Steel fibre content	kg/m^3	0, 40, 80

The concrete was mixed in a compulsory mixer with a nominal volume of 160 L. First, the cement and the aggregates were homogenized for 30 s before the water was added in the ongoing mix process. After a first mixing phase of two minutes, a visual inspection of the concrete was carried out and adhering components on the mixer wall were removed. Afterwards, the concrete was re-mixed for one minute before the consistency was tested via a flow table test. Additionally, the fresh concrete density and the air content were determined in accordance with EN 12350-5 [36], EN 12350-6 [37] and EN 12350-7 [38]. Fo the SFRC, the fibres were added subsequently and followed by another mixing period of at least one minute.

After the final mixing, six cylinders with included electrodes (see Section 2.2) were produced and compacted on a vibrating table. The specimens were covered with foil to avoid the dehydration of the surface. The specimens were left in the formwork and were stored in a climate of 20 °C and 65% relative humidity, since water storage was suspected to damage the electrical contacts of the electrodes. For each combination of fibre content and electrode array, one specimen was produced and tested. The small number of samples was chosen in order to gain the initial results of the new test setup and to investigate the general suitability of the newly developed method for the detection of fibre content and orientation. Therefore, a statistical analysis of the results was not possible and is planned to be performed in further investigations with a larger number of samples.

2.2. Experimental Setup

The basic setup from [33], consisting of two stainless steel electrodes with dimensions of 200 × 200 mm^2 connected to an LCR meter, was adjusted to enable the measurement of

cylindrical specimens. The LCR meter used for impedance measurements was an Extech Instruments LCR 200 with a voltage amplitude of 600 mV rms and variable frequencies of the alternating current of 100 Hz, 120 Hz, 1 kHz, 10 kHz and 100 kHz.

For the investigation of the cylindrical specimens, an advanced test setup was developed based on the existing equipment. Therefore, as the first step, a breadboard (see Figure 1) was configured, including the LCR meter, which was directly connected to the different electrodes. With this approach, it was possible to analyse the electrical resistivity, which was calculated from the electrical resistance and the dimensions of the specimens in different directions inside the specimens.

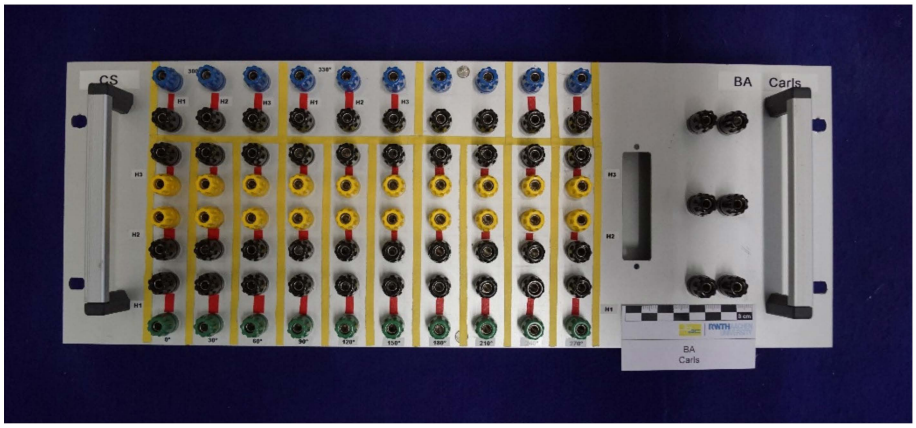

Figure 1. Breadboard for the connection of the LCR meter and different electrodes.

The setup was validated using cylindrical specimens with a height of 200 mm and a diameter of 100 mm with built-in metal oxide coated titanium (MMO) electrodes. Those electrodes were included in PVC formworks with a resulting connection area of 40 × 10 mm^2 each and could be connected via a notch to the breadboard from the outside. This setting was chosen in order to ensure a good connectivity between the electrodes and concrete and eliminate the effects of contact pressure. In total, six specimens with electrodes at three different heights with vertical distances of 20 mm each were prepared. Three of the specimens consisted of twelve electrodes with angular distances of 90° and the other three six electrodes with angular distances of 180°. The resulting formwork, consisting of twelve electrodes, and the electrodes themselves are presented in Figure 2.

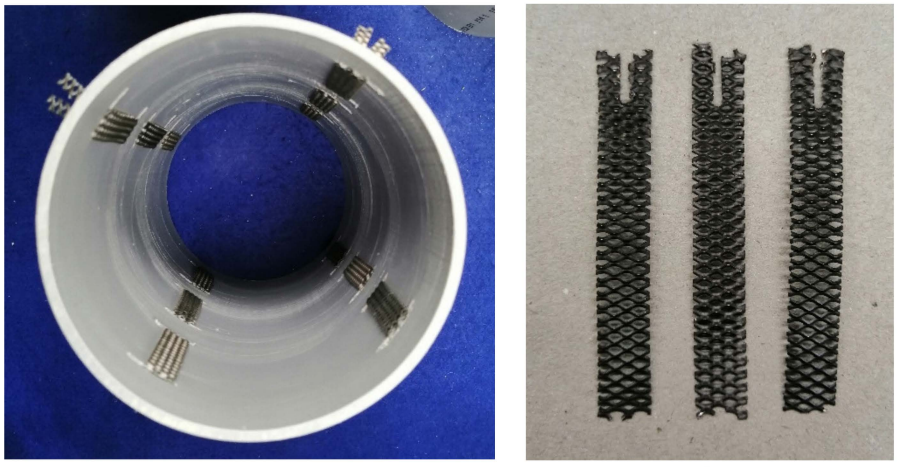

(**a**) (**b**)

Figure 2. PVC formwork with 12 MMO grid electrodes at three height levels with angular distances of 90° (**a**) and MMO grid electrodes with notches for the clamp (**b**).

2.3. Modelling of Current Flow

For the comparison of the resulting values of the measurements with the LCR meter, the electrical resistance must be converted to electrical resistivity considering geometry factors, which depend on the current flow. While the electrical resistivity, measured in Ωm, is a material-specific parameter and is free of any geometrical influences, the electrical resistance, measured in Ω, is a measurable value based on a specific configuration of the test setup and the specimen geometry. For trivial electrode configurations, such as two parallel plates, which have been used for the cubic specimens in earlier studies [33], this geometry factor is easy to calculate, but a simulation of the electrical current flow is necessary for more complex configurations. For this purpose, the software Comsol Multiphysics (version 5.3a, build version 229) was used and a grid model of the cylindrical specimens was generated.

The model consists of a cylinder with a diameter of 100 mm and a height of 200 mm and represents the concrete specimen. On the surface, there are 12 electrodes at three height levels, 4 on each level, in circular distances of 90° and with a thickness of 1 mm. Each electrode has an area of 40 × 10 mm^2 and is simulated as a segment of a circle to enable optimal connection to the cylinder. In this way, the model can be used for various electrode configurations. The FEM model of the test setup is presented in Figure 3a and the resulting grid model for a 12-electrode configuration can be seen in Figure 3b. The model presented was set up using the following assumption: the concrete and steel domain are considered to show homogeneous and isotropic behaviour and the sponge cloths as well as the polarization behaviour of the steel electrodes can be neglected. The latter is considered to be a valid assumption for the alternating current (AC) measurements using the parameters stated above.

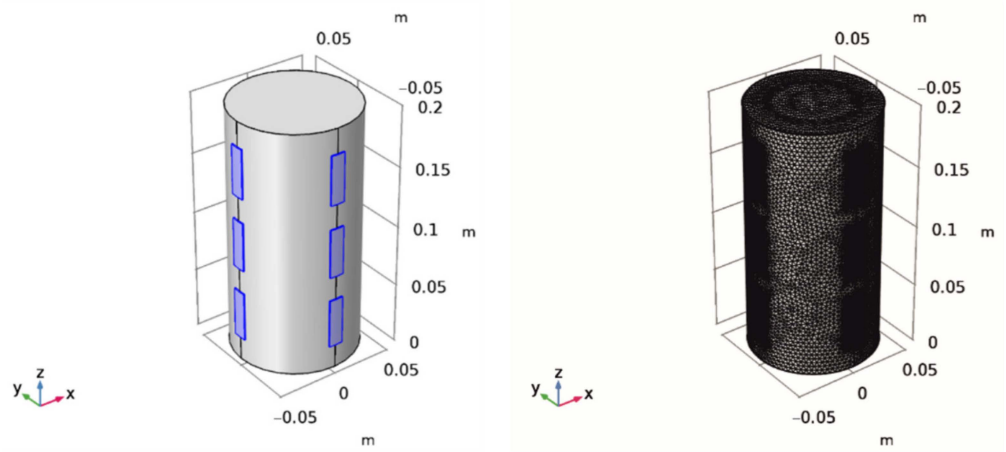

Figure 3. FEM model for cylindrical specimens consisting of a concrete cylinder (grey) and twelve electrodes (40 × 10 mm^2) at three height levels and with angular distances of 90 °C (blue) (**a**) and grid model to simulate current flow with an extremely fine grid (**b**).

With this model, the geometry factors (k) of all applied electrode configurations were determined assuming a specific material resistance for the concrete of 100 Ωm and an electric potential of 0 V for one electrode or set of parallel connected electrodes and 600 mV for the second electrode or set of parallel connected electrodes. Those values were chosen for the simulations as near realistic values for the test setup and materials (see Section 2.2). The simulations resulted in a calculated current by Comsol, which enabled the estimation of the geometry factor using Equation (1). The calculated k factors are mentioned in respective areas for each section of the results.

$$k = \frac{I * \rho}{U} \quad (1)$$

with k: the geometry factor in m

I: the electric current in A
ρ: the electrical resistivity (set to 100 Ωm)
U: the electric potential (set to 1 V)

Since the connection of the MMO grids, embedded in the concrete, illustrate a near optimal connection of electrodes and concrete, the electrical conductivity of the electrodes was set to that of titanium, for MMO, of 2.5×10^6 S/m. The visualisation in Figure 4a shows that unconnected electrodes (at the middle height level) have an impact on the iso-surfaces of the current, which represent locations with identical electric potential, in the case of a good electrical connection between the concrete and the electrodes. The current flow can be supposed to be orthogonal to those iso-surfaces. For the setup with a lower number of embedded electrodes with angular distances of 180°, Figure 4b shows that the iso-surfaces are more parallel in the parts of the specimen where no electrodes are embedded, but less uniformly distributed over the whole specimen. Additionally, for a horizontal current flow, the setup with electrodes with angular distances of 180°, only one direction (y) is measurable, while for the setup with a higher number of electrodes, both directions (x and y) can be analysed. In the later experiments, therefore, it is assumed that both horizontal directions have almost the same electrical resistivity and thus, the relative conductivity of different directions, representing the relative orientation of the fibres (orientation factor), can be calculated.

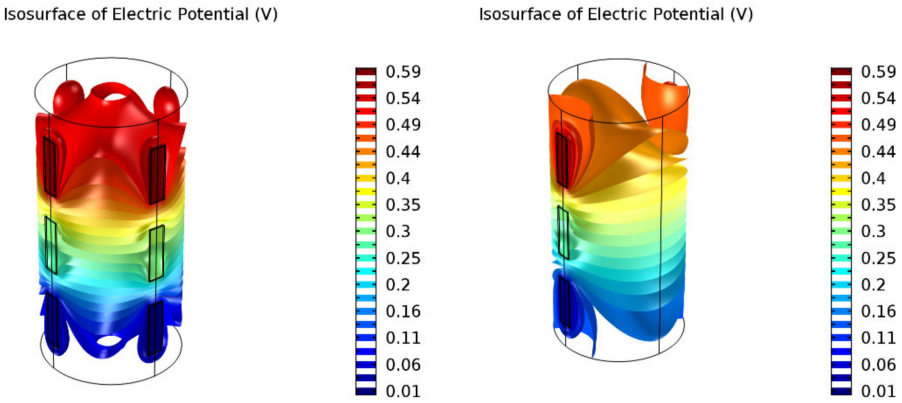

(**a**) (**b**)

Figure 4. Resulting iso-surfaces, calculated by Comsol, for angular distances of the electrodes of 90° (**a**) 180° (**b**).

2.4. Evaluation of the Results

After the calculation of the electrical resistivity of each electrode configuration was carried out, the fibre content and the fibre orientation inside the concrete were analysed using the equation of [5] (Equation (2)).

$$\frac{\sigma}{\sigma_m} = 1 + [\sigma]_\Delta * \Phi \tag{2}$$

with: σ: the electrical conductivity of the SFRC in Ωm
σ_m: the electrical conductivity of the PC in Ωm
Φ: the fibre volume fraction
$[\sigma]$: the intrinsic conductivity (Equation (3))
Δ: the ratio of conductivity of fibres and PC

For steel fibres, the ratio of conductivity of the fibres and plain concrete Δ tends to infinity, so the intrinsic conductivity can be calculated as follows [5]:

$$[\sigma]_{\infty} = \frac{1}{3}\left(\frac{2 * (AR)^2}{3 * ln[4(AR)] - 7} + 4\right) \quad (3)$$

with: AR: the aspect ratio of the fibres

For the given aspect ratio of 60, an intrinsic conductivity of 255.5 can be calculated. By converting Equation (2), the fibre content can be directly determined from the results of the measurements. Therefore, for all types of specimens, a global value of electrical resistivity respectively conductivity has to be determined. For the cylindrical specimens, several combinations were tested to find the optimum result.

When Equation (2) is used with the single direction test results of only one electrode configuration, it can be used to estimate the fibre orientation of this direction in context to the whole specimen by building the ratio to the sum of the other directions or three times the global fibre content.

3. Results and Discussion

3.1. Validation of the Test Setup

3.1.1. Impact of the Frequency of the Alternating Current

In the first series of six specimens, one of each fibre content and electrode array, with fibre contents of 0, 40 and 80 kg/m^3, the test setup was assessed in combination with the FEM model, where the electrical conductivity of the electrodes was set to that of titanium (2.5×10^6 S/m). The corresponding geometry factors are given in Tables A1 and A2 in Appendix A. The specimens were left covered with foil in the formworks and were tested at 9 days and 38 days of age. The different test dates were chosen to see whether changes in the pore structure of the concrete, based on hydration, show significant influences on the results of the electrical resistivity measurements. The age of 9 days represents a very early stage of the concrete, where the hydration process has not yet been finished but an initial investigation of concrete structures would be possible because partial demoulding could be performed, depending on the structure itself. The age of 38 days was chosen because it was assumed that the hydration process would be almost complete and the drying process of the concrete should not have taken place, so a comparison of the results of both ages will provide information about the influence of the hydration process and will not be affected by the different saturation of the specimens. For each specimen, the electrical resistivity in the horizontal and vertical direction was determined with several electrode configurations and the five possible frequencies of the alternating current (100 Hz, 120 Hz, 1 kHz, 10 kHz, 100 kHz). As presented in several previous studies (see, e.g., [5,33]), the frequency of the alternating current influenced the electrical resistivity, where a higher frequency led to slightly lower resistivity values. While for the PC there was almost no influence and a change in frequency from 100 Hz to 100 kHz only resulted in a decrease in the resistivity of about 2 %, for SFRC, depending on the fibre content, a decrease of 10 to 20% was observed (see Figure 5).

To identify effects based on the specimen's direction, the age of the specimen and the number of electrodes inside the specimen, the calculated resistivity of the concrete, based on a measurement with an alternating current frequency of 1 kHz, was used throughout the study. With this approach, we were able to exclude polarisation and induction effects. Afterwards, the results of all frequencies were evaluated according to Section 2.4 to estimate the fibre content and the orientation of fibres inside the specimen.

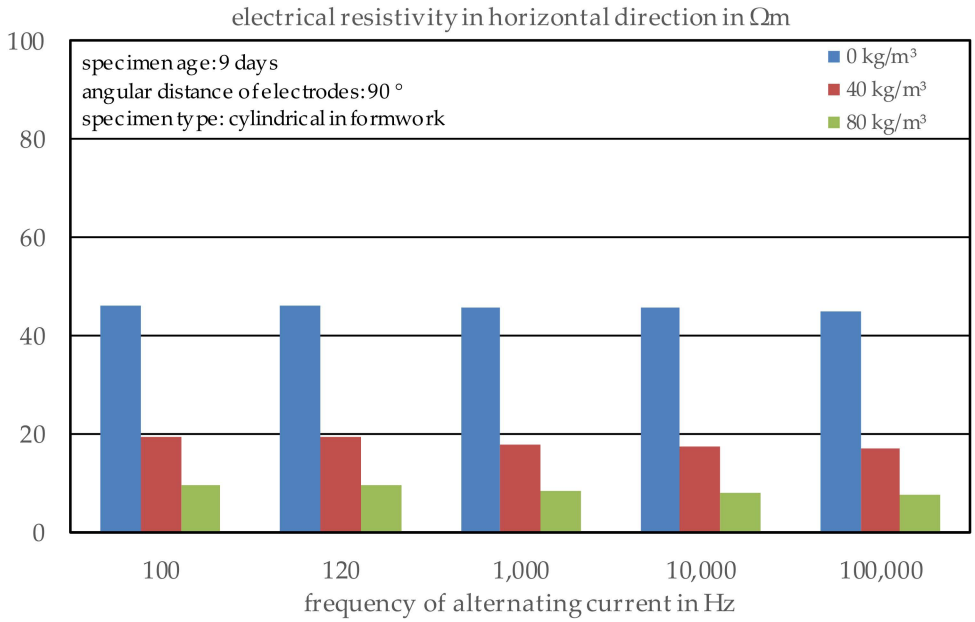

Figure 5. Electrical resistivity in the horizontal direction depending on the frequency and fibre content at a specimen age of 9 days and an electrode array with angular distances of 90°.

3.1.2. Electrode Array with Angular Distances of 180°

The results of the three specimens with an electrode array of only six electrodes with angular distances of 180° show that a higher fibre content results in a lower electrical resistivity of the composite material (see Figure 6), which is in line with several studies (see, e.g., [30,39–41]). This behaviour is the same for every direction that was analysed within this study. In the horizontal direction, the maximum area that was possible to analyse was investigated using a parallel connection of the electrodes at all three height levels on each side of the specimen (blue column). Compared to the measurements of single electrodes in the horizontal direction (red column) which means that the electrical resistance between both electrodes at height level one, level two and level three was measured, there is almost no difference in the electrical resistivity of the plain concrete, while for the fibre reinforced concretes, higher differences were observed. This can be explained by the inhomogeneity of the concrete and fibres and the anisotropy of the fibres, which are of a higher consequence if a smaller volume of materials is analysed.

For the electrical resistivity in the vertical direction, the same behaviour is detected, with higher electrical resistivities of the single electrode measurements (violet column) compared to the full area measurements (green column). Here, the full area measurements were performed using a parallel connection of each of the two electrodes at a height level and the current flow to the electrodes on another height level, while the single electrode measurements were based on a vertical current flow from one electrode to the other on the same side of the specimen at another height level. The slightly higher resistivity in the vertical direction, which can be seen for the fibre reinforced concretes, is probably caused by the compaction of the concrete on the vibrating table, which leads to the preferred orientation of the fibres in the horizontal direction and thus, an increased conduction ability in the horizontal direction.

When comparing the results of the same specimens at the age of 38 days (see Figure 7), it can be observed that the higher age of the concrete leads to a higher electrical resistivity, which is based on the development of the pore structure that gets finer through a higher degree of hydration. This effect is already described in several studies (see, e.g., [42–45]). In addition, as a result of the storage conditions, the drying process of the concrete itself takes place, which results in a lower pore saturation and thus, also increases the electrical resistivity of the concrete (see, e.g., [31,46,47]). Since the aging effect seems to be almost

constant for all fibre contents with an increase in resistivity of about 50%, it can be stated that the age or condition of the concrete must be identified to enable a prediction of the fibre content, while the fibre orientation, vertical and horizontal, can be estimated independent of the concrete.

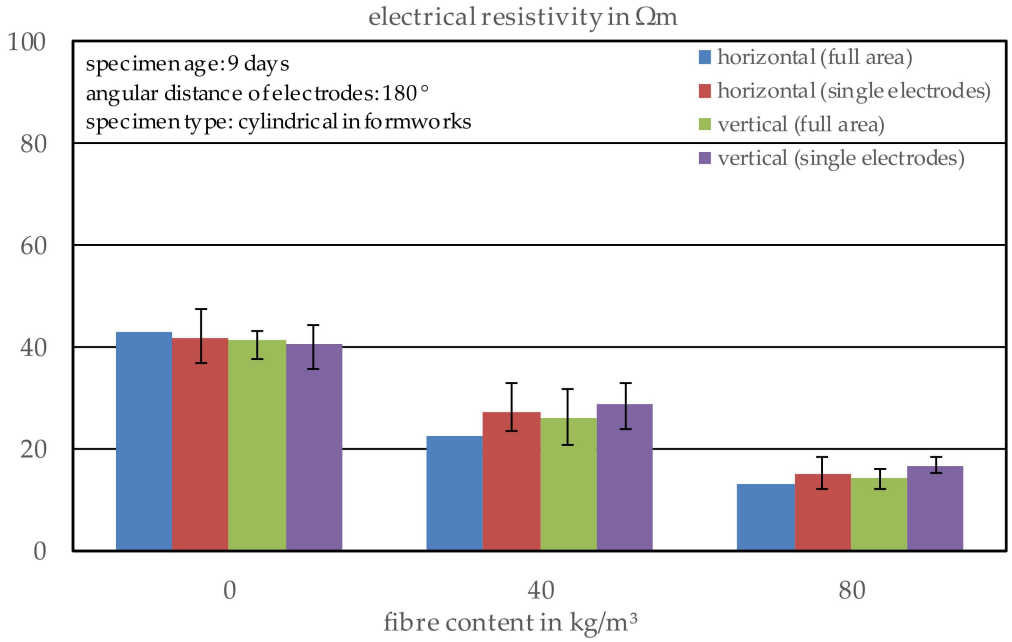

Figure 6. Electrical resistivity in different directions depending on fibre content at a specimen age of 9 days and an electrode array with angular distances of 180°.

3.1.3. Electrode Array with Angular Distances of 90°

The second series of three specimens was produced with four electrodes at each height level, corresponding to angular distances of 90° and so, more electrode arrays for the measurement were possible (see Figures 8 and A1 in Appendix A). According to the investigations described above, the electrical resistivities in the horizontal and vertical direction were determined too. For the plain concrete, it is again visible that the electrical resistivity in both directions is almost identical, while for the fibre reinforced concrete, especially with a fibre content of 40 kg/m^3, the resistivity in the vertical direction is higher than that in the horizontal direction. For the specimens with a higher fibre content, this phenomenon is not visible at the age of 9 days, while at a specimen age of 38 days, the maximum values of the resistivity in the vertical direction are at least higher than those in the horizontal direction. Nevertheless, based on the higher fibre content, a more three-dimensional fibre distribution and orientation can occur and so, the differences in the horizontal and vertical directions will be exalted at medium fibre contents, such as 40 kg/m^3.

Again, a higher concrete age leads to a higher variation that is caused by differences in the hydration and drying of the different parts of the specimens, where the outer surface shows the fastest drying process and the core of the sample has the highest saturation over time (see Figure A1 in Appendix A).

3.1.4. Evaluation of the Electrode Arrays

When comparing both electrode arrays, it can be noticed that for the plain concrete, the calculated resistivity of the array with angular distances of 90° was slightly higher, while for the fibre reinforced concretes, lower values were determined. Since the setup with more electrodes was able to describe the concrete in more detail and thus, different measuring directions were able to be analysed, the variations of the single electrode measurements, especially, but also of the full area measurements were higher than for the setup with a

lower number of electrodes (see Figures A2–A5 in Appendix A). The differences in the total results could be based on the variations of the single specimens but could also imply that the FEM model is not perfectly befitting of the test setup. A comparison of the single results of the measurements of both series was carried out to evaluate whether the differences between both test series could be a result of the FEM model. In evaluations up to now, it was assumed that all electrodes have a very good connection to the concrete and thus, no initial resistance occurs, but only the resistivity of the composite material has an influence on the measured electrical resistance.

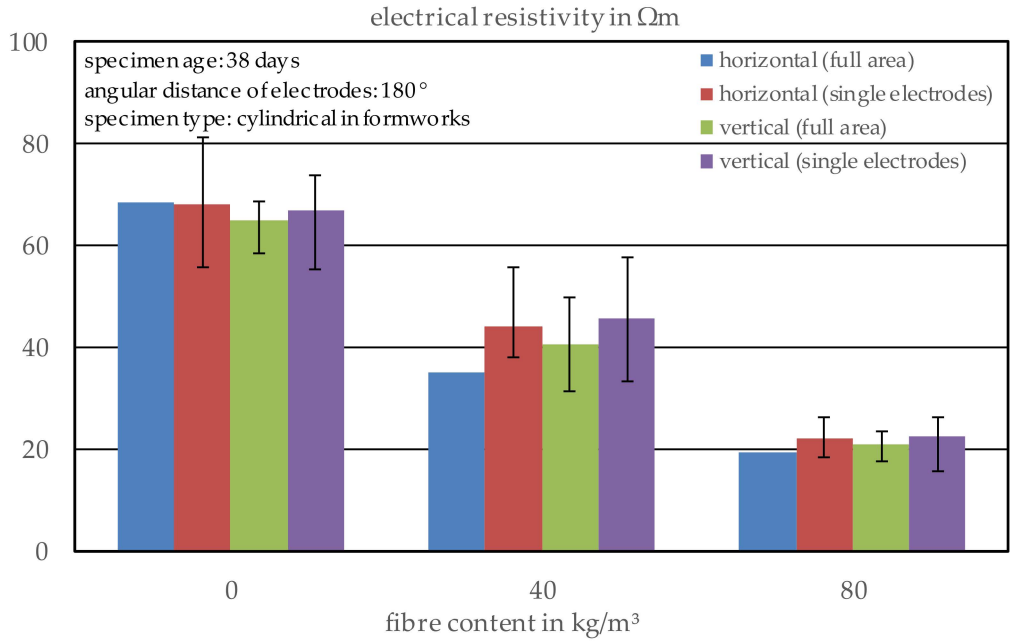

Figure 7. Electrical resistivity in different directions depending on fibre content at a specimen age of 38 days and an electrode array with angular distances of 180°.

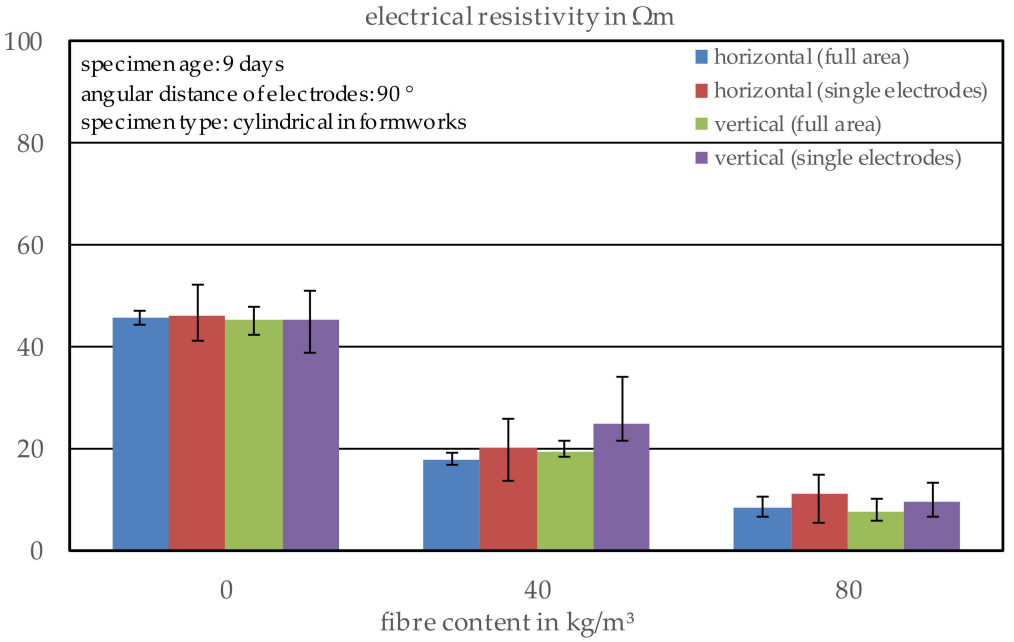

Figure 8. Electrical resistivity in different directions depending on fibre content at a specimen age of 9 days and an electrode array with angular distances of 90°.

To decide whether there is a general problem with the FEM model, the comparison of two different specimens can indeed offer a hint but cannot be seen as an absolute validation. So, the fact that, for the 90° electrode array, all values for the fibre reinforced concrete specimens were lower than for the other electrode array is no proof that the FEM model is not suitable just because the opposite behaviour is identified in the plain concrete.

As both electrode arrays consisted of three height levels of electrodes, the easiest way to identify the possible weaknesses of the model is to analyse the resistivity in the vertical direction. Here, three possibilities of the current flow are feasible: from height level one to height level two; from height level two to height level three; and from height level one to height level three. In this way, the percolated volume of the measurement from height level one to height level three should contain both volumes of the other measurements and thus, the resistivity will be approximately the mean value of the resistivities of both other combinations.

For the specimens with angular distances of the electrodes of 180°, the expected behaviour was almost identified for the PC and perfectly identified for the SFRC with a steel fibre content of 40 kg/m^3 (see Figure 9). In addition, the electrical resistivity from height level one to height level two, which represents the lower part of the specimen, was higher than the other values. This can be explained by an increased fraction of large aggregates and a lower porosity, based on the rise of water in the wet condition of the specimen as part of a small segregation process, even if the mixture was very stable. Only the specimen with a high fibre content the resistivity that was measured from the lowest to the highest height level of electrodes did not fit the expectations, but based on the high fibre content, it can be presumed that vertically orientated fibres in the middle area of the specimen could have a huge impact on the resistivity and thus, explain this result. Another explanation could be an increased number of short circuits as a result of the contact between a vertically oriented fibre and an electrode at height level two. The specimens with the second electrode array, with angular distances of 90°, showed the same tendency, where the expected behaviour could not be detected for the highest fibre content only (see Figure 10). In combination with the fact that the total resistivity for PC was smaller for the specimens tested with electrodes with angular distances of 180°, while for the SFRC the opposite behaviour was observed, and the changes in the electrical conductivity of the electrodes in the model did not lead to significant changes in the results, the conclusion was drawn that the small number of specimens was the reason for the partially unexpected results and thus, the model is probably applicable for a larger test series of drilling cores.

Nevertheless, based on the results of the validation series, the fibre contents of the single specimens and the fibre orientations inside the specimens were calculated using Equation (2) (see Section 2.4). For this purpose, each series of three specimens, the first with six electrodes with angular distances of 180° and the second with twelve electrodes with angular distances of 90°, was analysed separately. For the specimens with only six electrodes, only one horizontal direction of the specimens was tested, so it was assumed that the other direction was almost identical and that the global value of the resistance was calculated as the mean value of the vertical resistivity and two times the horizontal resistivity. For the specimens with twelve electrodes, both horizontal directions were used for the calculation of the global value. Due to the influence of the embedded electrodes at height level two on the vertical current flow, the vertical resistivity was calculated as the mean value of the vertical arrays from level one to level two, level one to level three and level two to level three to prevent any direct connections between the fibres and the electrodes and thus, a short circuit. Each plain concrete specimen was used as the reference for the conductivity of the matrix for the corresponding SFRC specimens.

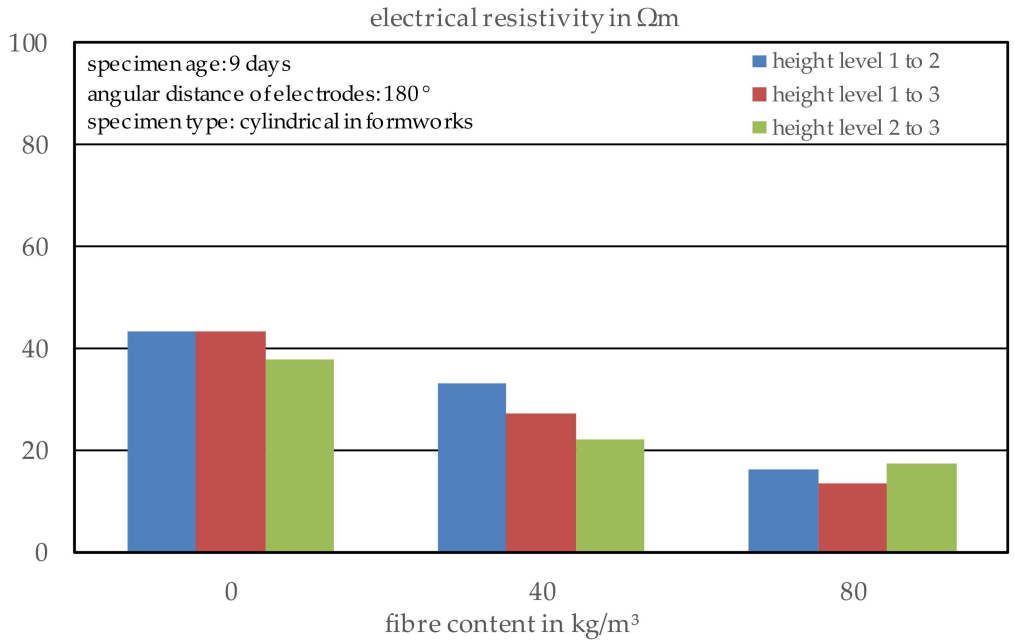

Figure 9. Electrical resistivity in the vertical direction with different combinations of electrodes depending on fibre content at a specimen age of 9 days and an electrode array with angular distances of 180°.

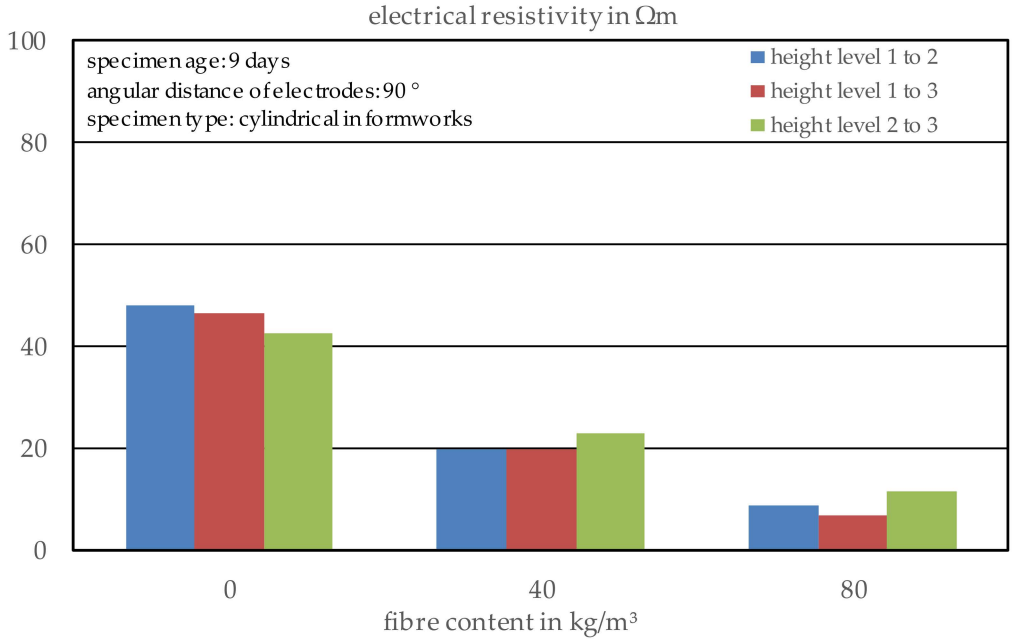

Figure 10. Electrical resistivity in the vertical direction with different combinations of electrodes depending on fibre content at a specimen age of 9 days and an electrode array with angular distances of 90°.

3.2. Estimation of the Fibre Content

As can be seen in Figure 11, the calculated fibre contents for both electrode arrays were not satisfactory. Only in two cases was a good estimation possible. The first case was an electrode array with angular distances of 180° for a fibre content of 40 kg/m^3 and low frequencies of the alternating current. The second case was an electrode array with angular distances of 90° for a fibre content of 80 kg/m^3 and high frequencies of the alternating current. In all other cases, the calculated results did not correspond to the produced

concrete. It is obvious that the fibre content is underestimated by the array with more electrodes, while the concrete with 80 kg/m^3 is strongly overestimated by the array with angular distances of 180°. Independent of fibre content and electrode array, the frequency of the alternating current showed an effect on the calculated results, where a higher frequency resulted in a higher fibre content. This is because without knowing the phase angle of the impedance, which cannot be detected with this test setup, it is not possible to determine the real part of the impedance and thus, based on those results, it is not possible to evaluate the possibility of determining the fibre content via the electrical conductivity. For a higher specimen age, the tendency is almost the same, while all calculated fibre contents are increased by 5 to 15% (see Figure A6 in Appendix A), the electrode array with angular distances of 90° provides a large discrepancy between the results and expectations and the results become better fitting for the other electrode array.

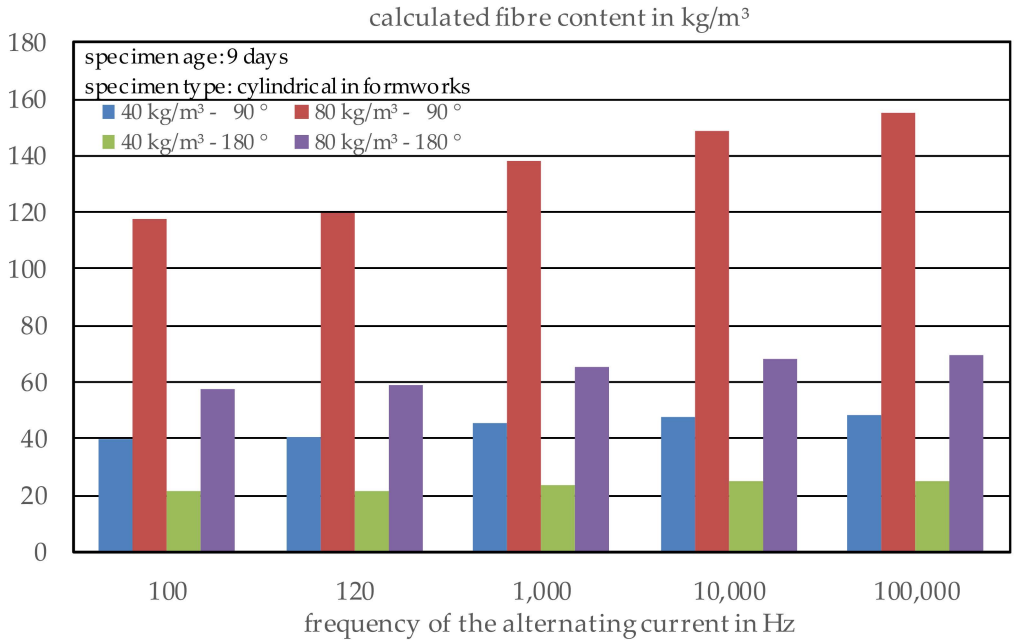

Figure 11. Calculated fibre content of the concrete specimens with different electrode arrays depending on fibre content and frequency of the alternating current at a specimen age of 9 days.

3.3. Estimation of the Fibre Orientation

According to the procedure described in Section 2.4, the fibre orientation inside the specimen was calculated. For the electrode array with angular distances of 90°, the orientation in two orthogonal horizontal directions and the vertical direction was possible, while for the setup with angular distances of 180°, it was only possible to measure one horizontal direction and it was assumed that the other horizontal direction would show the same value.

It was presumed that SFRC compacted by a vibrating table would show a higher number of fibres oriented in the horizontal direction than the vertical and, as Figure 12 shows, the calculations absolutely support this expectation for an alternating current frequency of 1 kHz, except for the specimen with 80 kg/m^3 of fibres and an electrode array with angular distances of 90°. Changes in the frequency did not lead to any important changes in the results. For most of the specimens, at a specimen age of 9 days, the calculation orientation factor in the horizontal direction was lower than that in the vertical direction. For the specimens with an electrode array of electrodes with angular distances of 90° it was observed that one horizontal direction always provided the highest calculated orientation and the other horizontal direction provided the lowest, while the vertical direction had an orientation factor of about 30–35%. For the specimens with angular distances of 180°, high orientation factors for the horizontal direction of more than 35% were calculated.

This could confirm the expectations but could also be a random result, because only one horizontal direction was investigated and, as the results of the investigations with more electrodes show, one horizontal direction could have very high orientation factors.

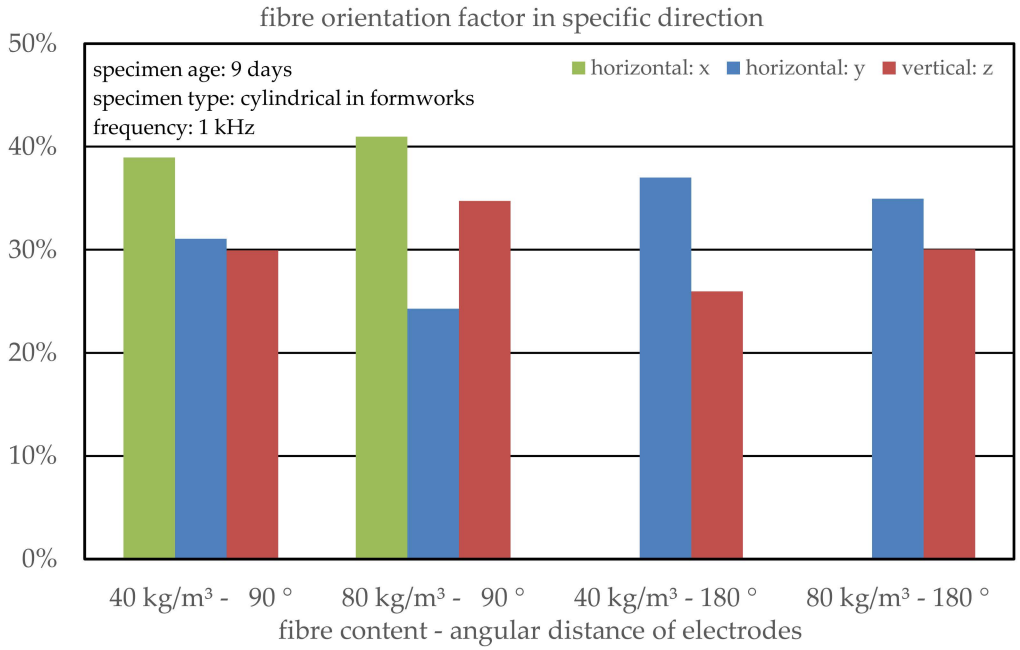

Figure 12. Calculated fibre orientation of the concrete specimens with different electrode arrays depending on fibre content at a specimen age of 9 days.

Comparing the results of the same specimens investigated at a concrete age of only 38 days, there were only small differences (see Figure A7 in Appendix A). It was concluded that the ongoing hydration process and thus, the pore structure in different parts of the specimen, would differ slightly based on small variations in the local water and cement content and so, lead to small variations in the calculated orientations for different concrete ages. While for the calculation of the fibre content, there was almost no influence of aging since the whole specimen was considered in its entirety for the calculation of the fibre content.

4. Conclusions

In summary, the test setup, consisting of a breadboard and a LCR meter, can be used for the analysis of both plain concrete and fibre reinforced concrete, and the FEM model provides the possibility to calculate the resistivity of the material and thus, to compare the different directions of the specimens. The evaluation of the specimens, included in formworks with electrodes, showed that the FEM model fits the real current flow inside the whole test setup, although the small number of specimens did not allow for a detailed analysis. While the age of the specimen, as well as the frequency of the alternating current, showed an impact on the calculated fibre content, neither parameter have any effect on the fibre orientation. The results show that with the increasing age of the concrete, the electrical resistivity also increases. For plain concrete, it increases from about 40 Ωm to 70 Ωm from 9 days to 38 days, but the proportion between steel fibre reinforced concrete and plain concrete is not affected because the electrical resistivity of the steel fibre reinforced concrete shows a proportionally smaller increase for a fibre content of 80 kg/m^3, based on the conductivity of the fibres.

Since the setup with angular distances of 90° allowed the analysis of specimens in at least three directions without the repeated mounting and demounting of the specimen, it was decided to use this number of electrodes and check which electrical resistivity of the electrodes showed the best results in the FEM model for further tests with drilling core

samples. The electrical parameters of the electrodes should be varied between the electrical resistivity of steel, to represent a good connection between the electrode and concrete, and the electrical resistivity of concrete, so a low connection could be analysed. With help of the developed test setup and the FEM model, a comparison between cubic specimens and drilling cores is part of current investigations being conducted by the authors [34] to validate the suitability of the setup for in situ analyses of existing structures.

Author Contributions: Conceptualization, methodology, validation, formal analysis, investigation, data curation, visualization, writing—original draft preparation: S.C. Review and editing, supervision and advice: T.M. and M.R. All authors have read and agreed to the published version of the manuscript.

Funding: This research received no external funding.

Institutional Review Board Statement: Not applicable.

Informed Consent Statement: Not applicable.

Data Availability Statement: The data presented in this study are available on request from the corresponding author. The data are not publicly available due to ongoing project work.

Conflicts of Interest: The authors declare no conflict of interest.

Appendix A

Table A1. Geometry factors k for the validation tests of the test setup, calculated by Comsol, with an electrode array with angular distances of 180° and the electrical conductivity of the electrodes in Comsol model of titanium of 2.5×10^6 S/m.

Electrode A		Electrode B		K-Value
Height Level	Angle	Height Level	Angle	
all	0°	all	180°	0.073252
1	0°	1	180°	0.026695
3	0°	3	180°	
2	0°	2	180°	0.026986
1	all	2	all	0.051199
2	all	3	all	
1	all	3	all	0.036845
1	0°	2	0°	0.027577
1	180°	2	180°	
2	0°	3	0°	
2	180°	3	180°	
1	0°	3	0°	0.021785
1	180°	3	180°	

Table A2. Geometry factors k for the validation tests of the test setup, calculated by Comsol, with an electrode array with angular distances of 90° and the electrical conductivity of the electrodes in Comsol model of titanium of 2.5×10^6 S/m.

Electrode A		Electrode B		K-Value
Height Level	**Angle**	**Height Level**	**Angle**	
all	0°	all	180°	0.072101
all	90°	all	270°	
1	0°	1	180°	0.026855
1	90°	1	270°	
3	0°	3	180°	
3	90°	3	270°	
2	0°	2	180°	0.027489
2	90°	2	270°	
1	all	2	all	0.086723
2	all	3	all	
1	all	3	all	0.054244
1	0°	2	0°	0.027987
1	90°	2	90°	
1	180°	2	180°	
1	270°	2	270°	
2	0°	3	0°	
2	90°	3	90°	
2	180°	3	180°	
2	270°	3	270°	
1	0°	3	0°	0.021898
1	90°	3	90°	
1	180°	3	180°	
1	270°	3	270°	

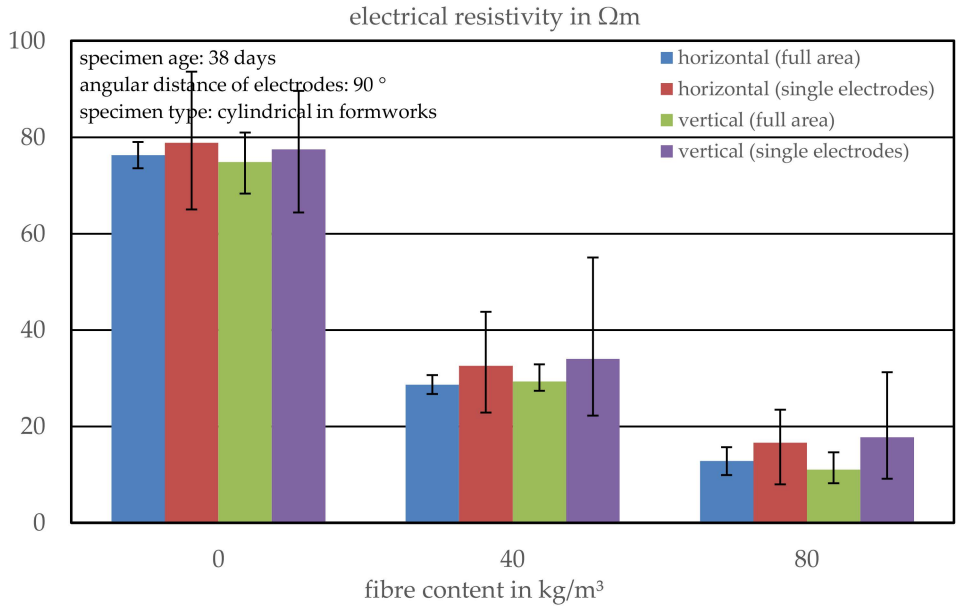

Figure A1. Electrical resistivity in different directions depending on the fibre content at a specimen age of 38 days and an electrode array with angular distances of 90°.

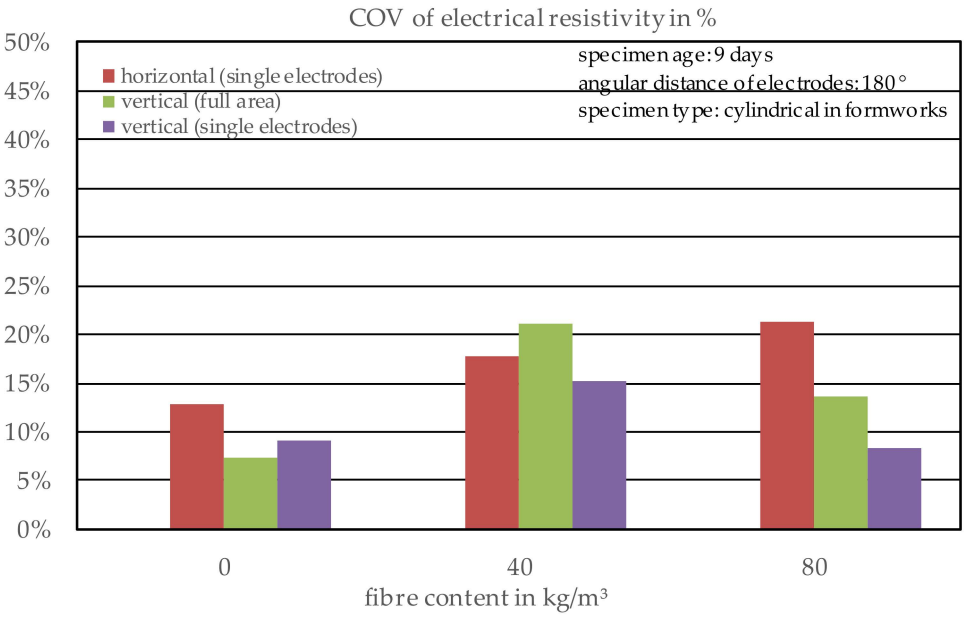

Figure A2. Coefficient of variation of the electrical resistivity in different directions depending on the fibre content at a specimen age of 9 days and an electrode array with angular distances of 180°.

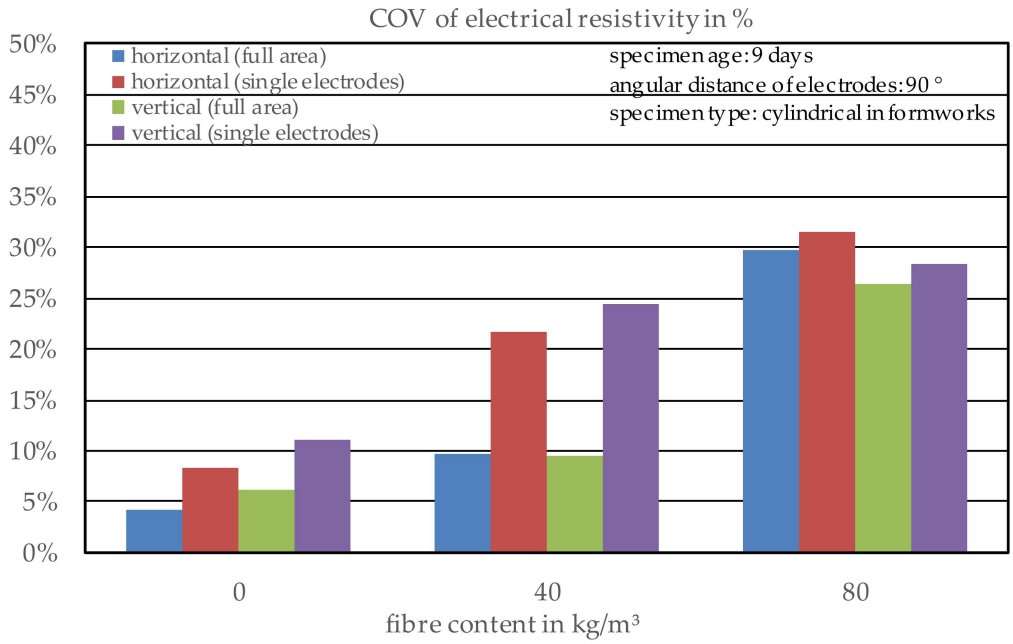

Figure A3. Coefficient of variation of the electrical resistivity in different directions depending on the fibre content at a specimen age of 9 days and an electrode array with angular distances of 90°.

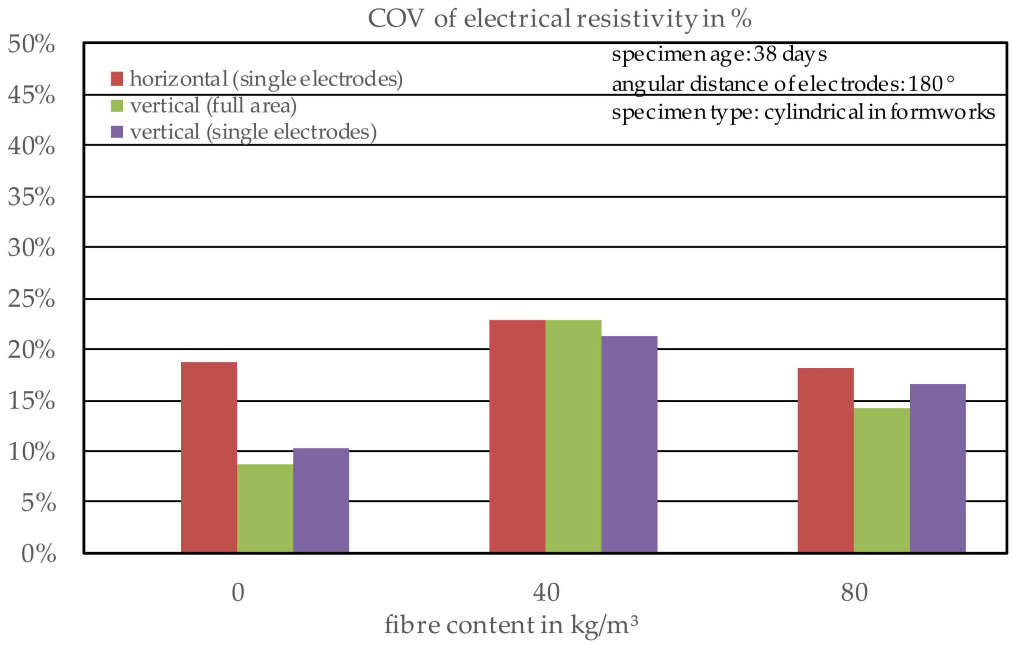

Figure A4. Coefficient of variation of the electrical resistivity in different directions depending on the fibre content at a specimen age of 38 days and an electrode array with angular distances of 180°.

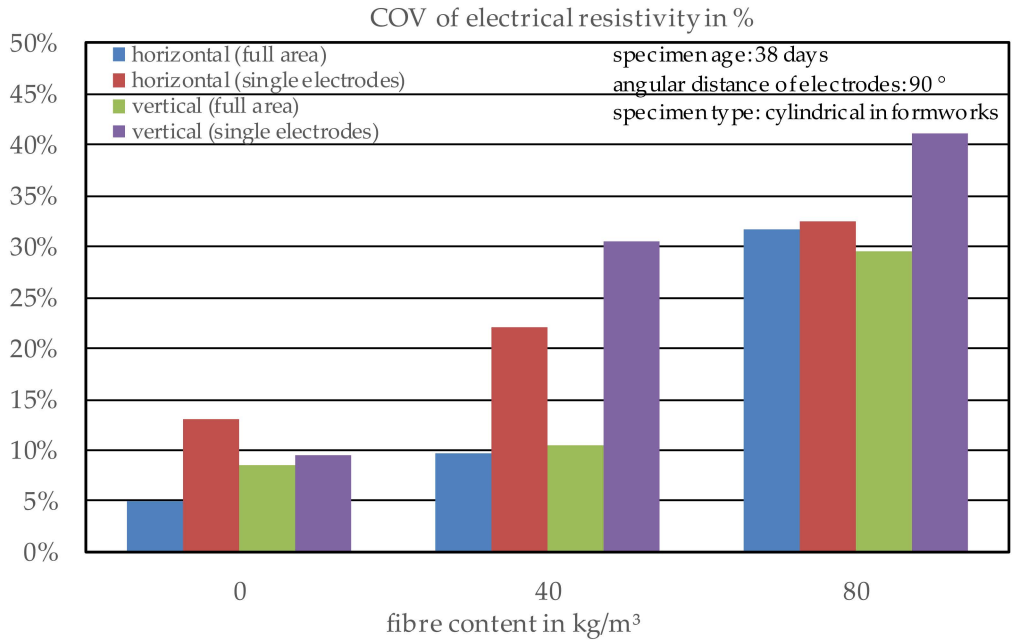

Figure A5. Coefficient of variation of the electrical resistivity in different directions depending on the fibre content at a specimen age of 38 days and an electrode array with angular distances of 90°.

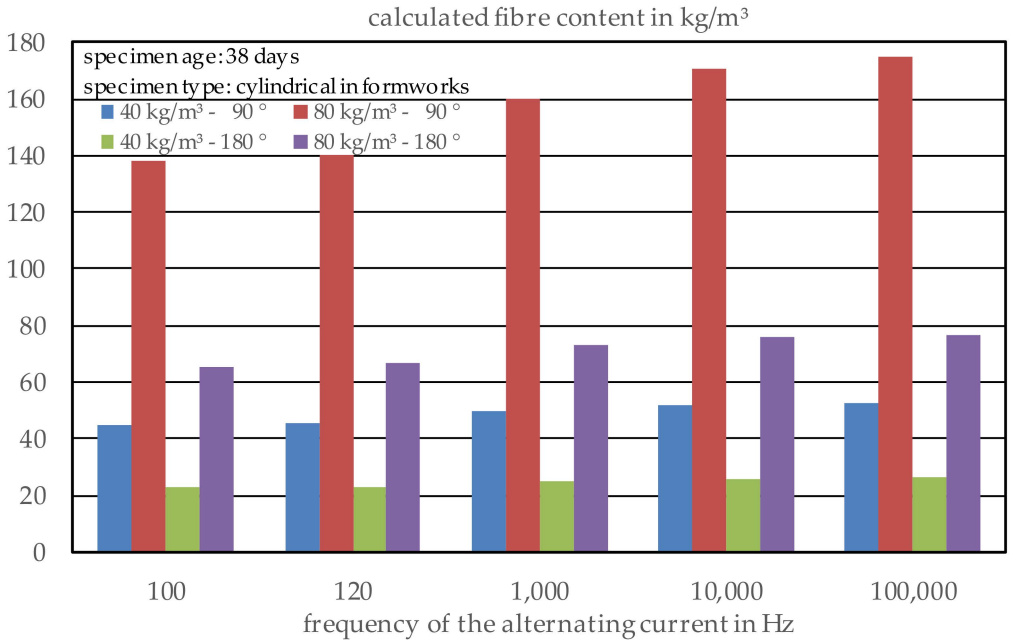

Figure A6. Calculated fibre content of the concrete specimens with different electrode arrays depending on the fibre content and frequency of the alternating current at a specimen age of 38 days.

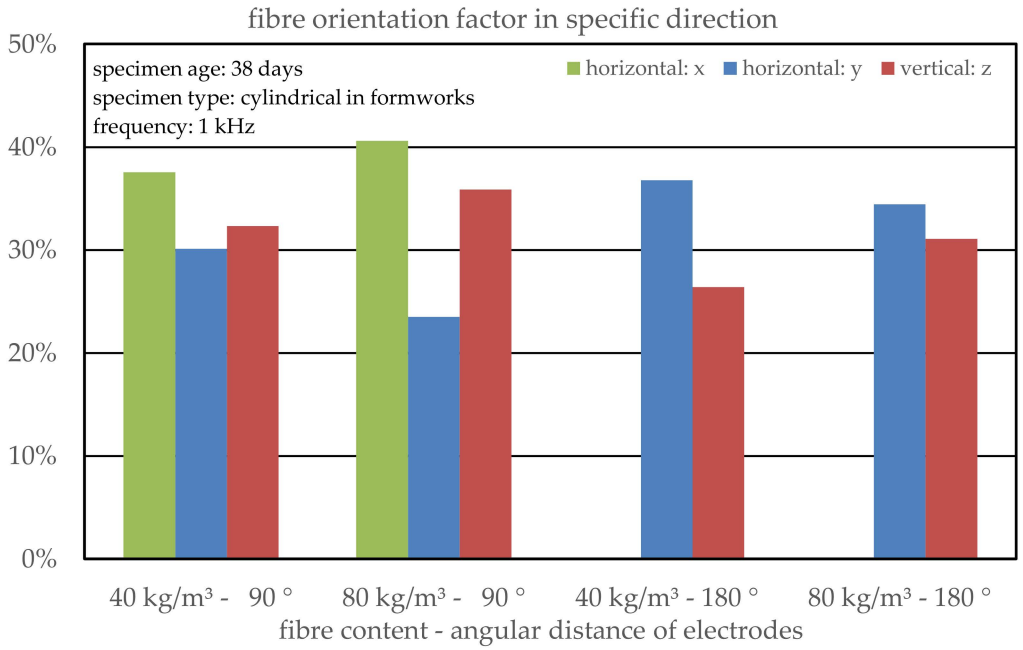

Figure A7. Calculated fibre orientation of the concrete specimens with different electrode arrays depending on the fibre content at a specimen age of 38 days.

References

1. Gouri Mohan, L.; Nazeer, M.; Nizad, A.; Suresh, S. Fibre reinforced concrete—A state-of-the-art review. *Int. J. Earth Sci. Eng.* **2010**, *3*, 634–642.
2. Kobaka, J.; Katzer, J.; Ponikiewski, T.A. Combined electromagnetic induction and radar-based test for quality control of steel fibre reinforced concrete. *Materials* **2019**, *12*, 3507. [CrossRef]
3. Luo, T.; Zhang, C.; Sun, C.; Zheng, X.; Ji, Y.; Yuan, X. Experimental investigation on the freeze–thaw resistance of steel fibers reinforced rubber concrete. *Materials* **2020**, *13*, 1260. [CrossRef]
4. Rossi, B.; Wolf, S. Steel fibre reinforced concrete for the future of tunnel lining segments—A durable solution. In *Tunnels and Underground Cities: Engineering and Innovation Meet Archaeology, Architecture and Art, Proceedings of the WTC 2019 ITA-AITES World Tunnel Congress, Naples, Italy, 3–9 May 2019*; CRC Press: Boca Raton, FL, USA, 2019; pp. 2978–2985. [CrossRef]
5. Woo, L.Y.; Wansom, S.; Ozyurt, N.; Mu, B.; Shah, S.P.; Mason, T.O. Characterizing fiber dispersion in cement composites using AC-Impedance Spectroscopy. *Cem. Concr. Compos.* **2005**, *27*, 627–636. [CrossRef]
6. Zhang, P.; Li, Q.; Chen, Y.; Shi, Y.; Ling, Y. Durability of steel fiber-reinforced concrete containing SiO_2 nano-particles. *Materials* **2019**, *12*, 2184. [CrossRef]
7. Gettu, R.; Gardner, D.R.; Saldívar, H.; Barragán, B.E. Study of the distribution and orientation of fibers in SFRC specimens. *Mater. Struct. Mater. Constr.* **2005**, *38*, 31–37. [CrossRef]
8. Martinelli, P.; Colombo, M.; Pujadas, P.; De la Fuente, A.; Cavalaro, S.; Di Prisco, M. Characterization tests for predicting the mechanical performance of SFRC floors: Identification of fibre distribution and orientation effects. *Mater. Struct.* **2021**, *54*, 3. [CrossRef]
9. Barnett, S.J.; Lataste, J.; Parry, T.; Millard, S.G.; Soutsos, M.N. Assessment of fibre orientation in ultra high performance fibre reinforced concrete and its effect on flexural strength. *Mater. Struct.* **2010**, *43*, 1009–1023. [CrossRef]
10. Zak, G.; Park, C.B.; Benhabib, B. Estimation of Three-Dimensional Fibre-Orientation Distribution in Short-Fibre Composites by a Two-Section Method. *J. Compos. Mater.* **2000**, *35*, 316–339. [CrossRef]
11. Plizzari, G.A. Fiber reinforced concrete for repairing and strengthening RC structures: Some recent advancements. In *Proceedings of the MATEC Web of Conferences*; EDP Sciences: Les Ulis, France, 2018; Volume 199, p. 01004. [CrossRef]
12. Cugat, V.; Cavalaro, S.H.P.; Bairán, J.M.; de la Fuente, A. Safety format for the flexural design of tunnel fibre reinforced concrete precast segmental linings. *Tunn. Undergr. Space Technol.* **2020**, *103*, 103500. [CrossRef]
13. Herrmann, H.; Boris, R.; Goidyk, O.; Braunbrück, A. Variation of bending strength of fiber reinforced concrete beams due to fiber distribution and orientation and analysis of microstructure. *IOP Conf. Series: Mater. Sci. Eng.* **2019**, *660*, 012059. [CrossRef]
14. Molins, C.; Aguado, A.; Saludes, S. Double Punch Test to control the energy dissipation in tension of FRC (Barcelona test). *Mater. Struct.* **2008**, *42*, 415–425. [CrossRef]
15. Tarawneh, A.; Almasabha, G.; Alawadi, R.; Tarawneh, M. Innovative and reliable model for shear strength of steel fibers reinforced concrete beams. *Structures* **2021**, *32*, 1015–1025. [CrossRef]

16. Komárková, T. Design of Methodology for Non-Destructive Testing of Steel-Reinforced-Fiber-Concrete. *Key Eng. Mater.* **2016**, *714*, 179–185. [CrossRef]
17. Li, L.; Xia, J.; Chin, C.; Jones, S. Fibre distribution characterization of ultra-high performance fibre-reinforced concrete (uhpfrc) plates using magnetic probes. *Materials* **2020**, *13*, 5064. [CrossRef]
18. Li, Y.; Ruan, X.; Akiyama, M.; Zhang, M.; Xin, J.; Lim, S. Modelling method of fibre distribution in steel fibre reinforced concrete based on X-ray image recognition. *Compos. Part B Eng.* **2021**, *223*, 109124. [CrossRef]
19. Woo, L.Y.; Kidner, N.J.; Wansom, S.; Mason, T.O. Combined Time Domain Reflectometry and AC-Impedance Spectroscopy of Fiber-Reinforced Fresh-Cement Composites. *Cem. Concr. Res.* **2007**, *37*, 89–95. [CrossRef]
20. Balázs, G.L.; Czoboly, O.; Lublóy, É.; Kapitány, K.; Barsi, Á. Observation of steel fibres in concrete with computed tomography. *Constr. Build. Mater.* **2017**, *140*, 534–541. [CrossRef]
21. Ferrara, L.; Faifer, M.; Toscani, S. A magnetic method for non destructive monitoring of fiber dispersion and orientation in steel fiber reinforced cementitious composites—Part 1: Method calibration. *Mater. Struct.* **2012**, *45*, 575–589. [CrossRef]
22. Lee, S.; Oh, J.; Cho, J. Fiber orientation factor on rectangular cross-section in concrete members. *Int. J. Eng. Technol.* **2015**, *7*, 470–473. [CrossRef]
23. Mattarneh, A.H. Electromagnetic quality control of steel fiber concrete. *Constr. Build. Mater.* **2014**, *73*, 350–356. [CrossRef]
24. Park, T.; Her, S.; Jee, H.; Yoon, S.; Cho, B.; Hwang, S.; Bae, S. Evaluation of orientation and distribution of steel fibers in high-performance concrete column determined via micro-computed tomography. *Constr. Build. Mater.* **2014**, *73*, 350–356. [CrossRef]
25. Ponikiewski, T.; Katzer, J. X-ray computed tomography of fibre reinforced self-compacting concrete as a tool of assessing its flexural behaviour. *Mater. Struct. Mater. Constr.* **2016**, *49*, 2131–2140. [CrossRef]
26. Torrents, J.M.; Blanco, A.; Pujadas, P.; Aguado, A.; Juan-García, P.; Sánchez-Moragues, M.Á. Inductive method for assessing the amount and orientation of steel fibers in concrete. *Mater. Struct.* **2012**, *45*, 1577–1592. [CrossRef]
27. Ozyurt, N.; Woo, L.Y.; Mason, T.O.; Shah, S.P. Monitoring Fiber Dispersion in Fiber-Reinforced Cementitious Materials: Comparison of AC-Impedance Spectroscopy and Image Analysis. *ACI Mater. J.* **2006**, *103*, 340–347.
28. Raupach, M.; Gulikers, J.; Reichling, K. Condition survey with embedded sensors regarding reinforcement corrosion. *Mater. Corros.* **2013**, *64*, 141–146. [CrossRef]
29. Reichling, K.; Raupach, M. Measurement and visualisation of the actual concrete resistivity in consideration of conductive layers and reinforcement bars. In *Concrete Repair, Rehabilitation and Retrofitting III, Proceedings of the 3rd International Conference on Concrete Repair, Rehabilitation and Retrofitting, Cape Town, South Africa, 3–5 September 2012*; Taylor Francis Group: Abingdon, UK, 2012; pp. 707–714.
30. Reichling, K. Bestimmung und Bewertung des Elektrischen Widerstands von Beton Mit Geophysikalischen Verfahren. Ph.D. Thesis, Technische Hochschule, Aachen, Germany, 2014.
31. Reichling, K.; Raupach, M.; Klitzsch, N. Determination of the distribution of electrical resistivity in reinforced concrete structures using electrical resistivity tomography. *Mater. Corros.* **2015**, *66*, 763–771. [CrossRef]
32. Ruan, T.; Poursaee, A. Fiber-distribution assessment in steel fiber-reinforced UHPC using conventional imaging, X-ray CT scan, and concrete electrical conductivity. *J. Mater. Civ. Eng.* **2019**, *31*, 04019133. [CrossRef]
33. Cleven, S.; Raupach, M.; Matschei, T. Electrical Resistivity of Steel Fibre-Reinforced Concrete—Influencing Parameters. *Materials* **2021**, *14*, 3408. [CrossRef] [PubMed]
34. Cleven, S.; Raupach, M.; Matschei, T. A New Method to Determine the Steel Fibre Content of Existing Structures—Evaluation and Validation. *Appl. Sci.* **2022**, *12*, 454. [CrossRef]
35. *EN 206:2013+A1:2016*; *DIN EN 206:2017-01*; Concrete-Specification, Performance, Production and Conformity; German Version. Beuth Publishing DIN: Berlin, Germany, 2017. [CrossRef]
36. *EN 12350-5:2019*; *DIN EN 12350-5:2019-09*; Testing Fresh Concrete—Part 5: Flow Table Test; German Version. Beuth Publishing DIN: Berlin, Germany, 2019. [CrossRef]
37. *EN 12350-6:2019*; *DIN EN 12350-6:2019-09*; Testing Fresh Concrete—Part 6: Density; German Version. Beuth Publishing DIN: Berlin, Germany, 2019. [CrossRef]
38. *EN 12350-7:2019*; *DIN EN 12350-7:2019-09*; Testing Fresh Concrete—Part 7: Air Content—Pressure Methods; German Version. Beuth Publishing DIN: Berlin, Germany, 2019. [CrossRef]
39. Chen, B.; Wu, K.; Yao, W. Conductivity of carbon fiber reinforced cement-based composites. *Cem. Concr. Compos.* **2004**, *26*, 291–297. [CrossRef]
40. Hedjazi, S.; Castillo, D. Effect of fibre types on the electrical properties of fibre reinforced concrete. *Mater. Express* **2020**, *10*, 733–739. [CrossRef]
41. Lataste, J.F.; Behloul, M.; Breysse, D. Characterisation of fibres distribution in a steel fibre reinforced concrete with electrical resistivity measurements. *NDT E Int.* **2008**, *41*, 638–647. [CrossRef]
42. Daniel, J.I.; Gopalaratnam, V.S.; Galinat, M.A.; Ahmad, A.H.; Hoff, G.C.; Arockiasamy, M.; Jindal, R.L.; Shah, S.P.; Balaguru, P.N. *Report on Fiber Reinforced Concrete. Reported by ACI Committee 544*; ACI544.1R-96; American Concrete Institute: Indianapolis, IN, USA, 2001.
43. Gjørv, O.E.; Øystein, V.; El-Busaidy, A.H.S. Electrical resistivity of concrete in the oceans. In Proceedings of the Offshore Technology Conference, Houston, TX, USA, 1–4 May 1977; Volume 2, pp. 581–588. [CrossRef]

44. Liu, Y.; Presuel-Moreno, F. Effect of elevated temperature curing on compressive strength and electrical resistivity of concrete with fly ash and ground-granulated blast-furnace slag. *ACI Mater. J.* **2014**, *111*, 531–542.
45. Spragg, R.; Jones, S.; Bu, Y.; Lu, Y.; Bentz, D.; Snyder, K.; Weiss, J. Leaching of conductive species: Implications to measurements of electrical resistivity. *Cem. Concr. Compos.* **2017**, *79*, 94–105. [CrossRef] [PubMed]
46. Andrade, C. Model for prediction of reinforced concrete service life based on electrical resistivity. *IBRACON Mater. J.* **2005**, *1*, 1–5.
47. Bürchler, D. Der Elektrische Widerstand von Zementösen Werkstoffen. Ph.D. Thesis, ETH Zürich, Zürich, Switzerland, 1996. [CrossRef]